Paper

Electric Field Calculation for Composite Dielectrics by a Curved Surface Charge Method with Non-conforming Charge Representation

Member Shoji Hamada (Department of Electrical Engineering, Kyoto University)
Member Tadasu Takuma (Department of Electrical Engineering, Kyoto University)
Member Yoshio Saitoh (High Energy Accelerator Research Organization (KEK))

This paper describes an improved surface charge method (SCM) that analyzes the electric field in composite dielectrics in a three-dimensional (3D) arrangement. In this SCM, curved boundary surfaces are represented by third-order shape representation functions, and surface charge density distributions on the surfaces are expressed by non-conforming first-order charge representation functions. This type of SCM realizes natural treatment of curved surfaces, and also numerically stable treatment of edge parts of the shapes and triple junctions of different materials without any additional modifications. Two benchmark-test calculations are carried out to confirm the validity of the proposed method. It has also been applied to field analysis for a real 3D dielectric support of a high voltage feed line.

Keywords: electric field, composite dielectrics, numerical calculation, surface charge method, non-conforming element

1. Introduction

Surface charge method (SCM) is a numerical field calculation technique, which simulates an electric field with the equivalent charge on the boundary surfaces. Although it has a long history of application, it is not yet fully developed as a reliable and accurate method, in particular, in composite dielectrics and three-dimensional conditions. We have been improving the accuracy of SCM in these conditions [1], [2] by applying various computational techniques relating to

(i) representation of surface profiles,

(ii) expression of charge density on boundary surfaces, and (iii) formulation of boundary conditions.

In this paper, we demonstrate the usefulness of a curved surface charge method with non-conforming charge representation. This type of SCM is realized by the following procedures.

(1) Control points of Bézier patches are defined, which express the third-order triangular and quadrilateral surfaces.

(2) Non-conforming first-order functions are prepared, which represent surface charge density distributions on the surface elements.

(3) Matching points of boundary conditions are defined, which give a set of linear equations to solve the unknown variables of surface charge density.

The following calculations are carried out, and the results are presented.

(A) Benchmark test I : Spherical dielectric.

(B) Benchmark test II : Cubic dielectric.

(C) Practical example : Dielectric support.

2. Formulation of SCM

2.1 Representation of surface profile When a model to be treated has a rounded shape, usage of a curved element is recommended in order to perform reliable field calculation. Some kinds of curved elements have been applied for such purposes in the high voltage engineering field [2] ~ [4]. Here, we use a triangular and a quadrilateral Bézier patches [5] whose sides are represented by Ferguson cubic curves [6].

For the triangular patch, we adopt the third-order shape functions proposed by Zienkiewicz [7]. For the quadrilateral patch, we adopt the third-order Serendipity shape functions [7]. These surfaces are numerically described by the formulation of the Bézier patch, and they are defined by the control points as shown in Fig. 1 and 2. In the figures, circles mean the control points. The position vectors of 'on-side' control points are determined directly from the Ferguson curves. For example, the following relationship is valid in Fig. 1.

$$\boldsymbol{x}_4 = \boldsymbol{x}_1 + \frac{1}{3}\boldsymbol{t}_{12} \ . \quad \cdots\cdots\cdots\cdots\cdots\cdots\cdots\cdots \quad (1)$$

where $\boldsymbol{x}$ means a position vector of a control point identified with a subscript number, and $\boldsymbol{t}$ means a tangent vector at the first subscribed node toward the second one. The Ferguson curves can be determined by simple procedures, for example, by the method described in reference [8], when the coordinates of vertices and the side-connection information are provided.

In Fig. 1, the position vector of an interior control point is calculated by the following equation.

$$\boldsymbol{x}_{10} = -\frac{2}{12}(\boldsymbol{x}_1 + \boldsymbol{x}_2 + \boldsymbol{x}_3) + \frac{3}{12}(\boldsymbol{x}_4 + \boldsymbol{x}_5 + \boldsymbol{x}_6 + \boldsymbol{x}_7 + \boldsymbol{x}_8 + \boldsymbol{x}_9) \ . \quad (2)$$

In Fig. 2, the position vectors of interior control points are calculated by the following way.

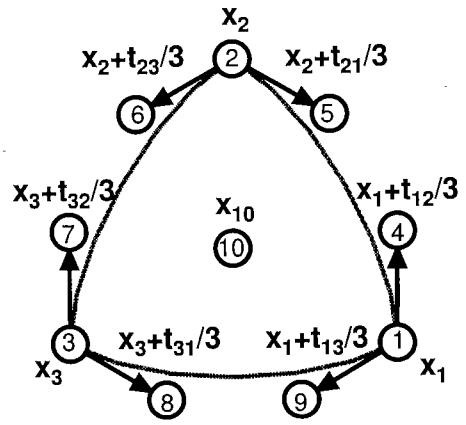

Fig. 1 Control points of the Bézier patch, which represent a Zienkiewicz triangular element.

$$\boldsymbol{x}_{13} = -\frac{4}{9}\boldsymbol{x}_1 + \frac{6}{9}(\boldsymbol{x}_5 + \boldsymbol{x}_{12}) - \frac{2}{9}(\boldsymbol{x}_2 + \boldsymbol{x}_4) + \frac{3}{9}(\boldsymbol{x}_7 + \boldsymbol{x}_{10}) - \frac{1}{9}\boldsymbol{x}_3 \ . \quad \cdots\cdots\cdots\cdots \quad (3)$$

$\boldsymbol{x}_{14}$, $\boldsymbol{x}_{15}$, and $\boldsymbol{x}_{16}$ are determined by the similar equations. The Bézier patch s is represented by the following formulations [5]. For a triangular element,

$$s(\xi_1, \xi_2, \xi_3) = \left(\xi_1 + E^{tri}\xi_2 + F^{tri}\xi_3\right)^3 \boldsymbol{x}_1 \ , \quad \cdots\cdots \quad (4)$$

where ξ_1, ξ_2, and ξ_3 mean area coordinates of a triangle, E^{tri} and F^{tri} mean the shift operators of the triangular control-point. E^{tri} and F^{tri} shift the operated control-point to the neighboring one in the ξ_2 and ξ_3 direction, respectively. For example, $E^{tri}\boldsymbol{x}_1$ means $\boldsymbol{x}_4$, $E^{tri}F^{tri}\boldsymbol{x}_1$ means $\boldsymbol{x}_{10}$, and so on. For a quadrilateral element,

$$s(\xi, \eta) = \left(1 - \xi + E^{quad}\xi\right)^3 \left(1 - \eta + F^{quad}\eta\right)^3 \boldsymbol{x}_1 \ , \quad (5)$$

where ξ and η ($0 \geq \xi, \eta \geq 1$) mean normalized coordinates, E^{quad} and F^{quad} mean the shift operators of the quadrilateral control-point. E^{quad} and F^{quad} shift the operated control-point to the neighboring one in the ξ and η direction, respectively. For example, $E^{quad}\boldsymbol{x}_1$ means $\boldsymbol{x}_5$, $E^{quad}F^{quad}\boldsymbol{x}_1$ means $\boldsymbol{x}_{13}$, and so on.

We use quadrilateral patches in most of the surfaces, and only partly use triangular patches.

2.2 Representation of a charge distribution

We use first-order shape functions to represent a charge density distribution on each element. For a triangular element, three shape functions agree with the area coordinates of a triangle. For a quadrilateral element, four shape functions are defined by the bi-linear function. These functions can also be expressed by the Bézier patch formulation. The charge density distribution σ is represented as follows. For a triangular element,

$$\sigma(\xi_1, \xi_2, \xi_3) = \left(\xi_1 + E^{tri}\xi_2 + F^{tri}\xi_3\right)\sigma_1 \ , \quad \cdots \quad (6)$$

and for a quadrilateral element,

$$\sigma(\xi, \eta) = \left(1 - \xi + E^{quad}\xi\right)\left(1 - \eta + F^{quad}\eta\right)\sigma_1 \ , \quad (7)$$

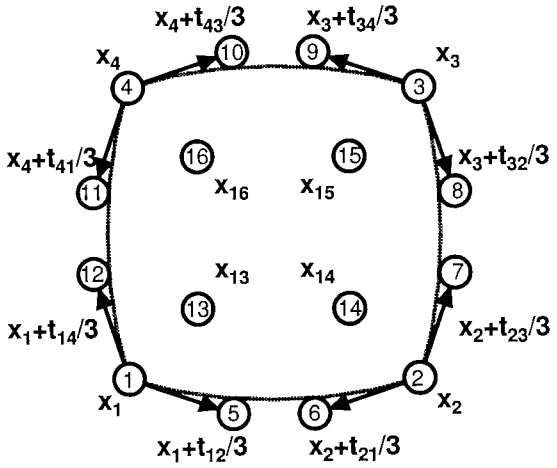

Fig. 2 Control points of the Bézier patch, which represent a Serendipity quadrilateral element.

where σ_1 means the charge density defined at $\boldsymbol{x}_1$. In eq. (6) and (7), the shift operators shift the control-point where σ is defined. For example, $E^{tri}\sigma_1$ means σ_2, $E^{quad}F^{quad}\sigma_1$ means σ_3, and so on.

In this calculation, the charge density distribution on the whole area is defined discontinuously at the all connecting-parts of element-sides, which is called the non-conforming element in the charge representation. In any case, the charge density distribution on each element is described by three or four charge density values at the triangular or quadrilateral vertices of the element, respectively.

2.3 Representation of boundary conditions

Boundary conditions are represented by a point matching method. When the point is on a conductor or dielectric surface, an equation for a potential or a normal component of flux density is needed there, respectively. For a triangular element, three matching points of boundary condition are required to harmonize with the three unknown variables. As these points, we choose the sampling points of a triangular area integration formula with three points [9]. The area coordinates (ξ_1, ξ_2, ξ_3) of these points are placed at $(\frac{4}{6},\frac{1}{6},\frac{1}{6})$, $(\frac{1}{6},\frac{4}{6},\frac{1}{6})$, and $(\frac{1}{6},\frac{1}{6},\frac{4}{6})$, respectively.

For a quadrilateral element, four matching points are required. As these points, we choose the sampling points of the Gauss integration formula with two points [7] in both ξ and η coordinates. The normalized coordinates (ξ, η) of these points are placed at (a,a), $(a,1-a)$, $(1-a,a)$, and $(1-a,1-a)$, respectively, where $a = 0.211325$.

3. Numerical results

3.1 Spherical dielectric As a benchmark example, we calculate the electric field for a spherical dielectric placed in the free space under a homogeneous field. As for this example, there exists the well-known analytical solution, so that we can easily examine the accuracy of the calculated results by comparing them with the analytical ones. And it is also known that the

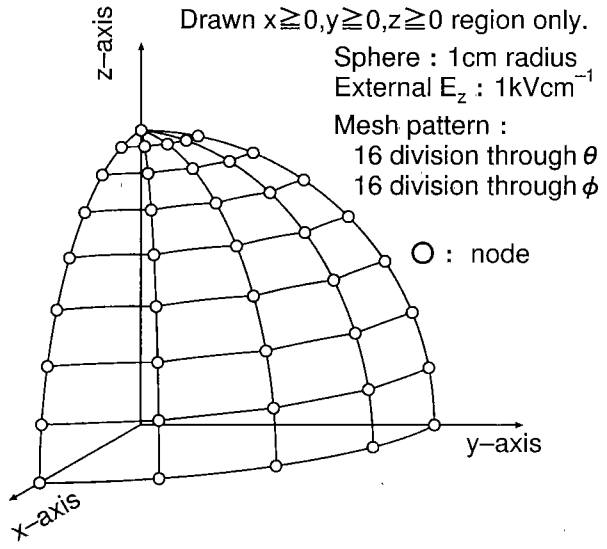

Fig. 3 Mesh pattern for a spherical dielectric.

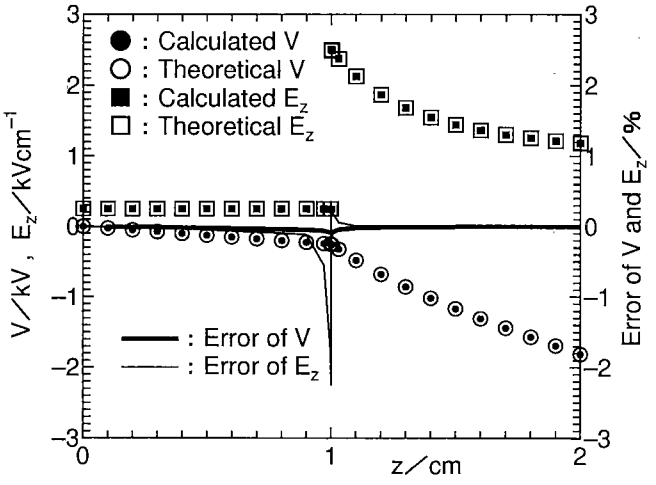

Fig. 4 Calculated potential V and field strength E_z on the z-axis for a spherical dielectric.

use of curved surface elements is quite necessary for a reliable numerical analysis of this case.

The radius of sphere, the relative permittivity, and the electric field strength are 1cm, 10, and 1kVcm^{-1} respectively. The homogeneous electric field is applied parallel to the z-axis. An example of applied mesh patterns is shown in Fig. 3. In this case, by counting a quadrilateral as two equivalent triangles, the number of equivalent triangular elements amounts to 480 over the entire surface. Fig. 4 shows the calculated potential V and electric field E_z on the z-axis corresponding to the mesh pattern of Fig. 3. Theoretical values and relative errors are also plotted in the figure. Inside the dielectric, the field error is less than about 0.1% . The maximum error of the field is -2.25% near the top of the dielectric (z=1 $-$ a cm, $a = 3 \times 10^{-6}$). We have also calculated the error of field strength in relation to the number of surface elements. Fig. 5 shows the calculated relative error (absolute value) of E_z at $z = 0$ and $z = 1-a$ in relation to the number of equivalent triangular elements.

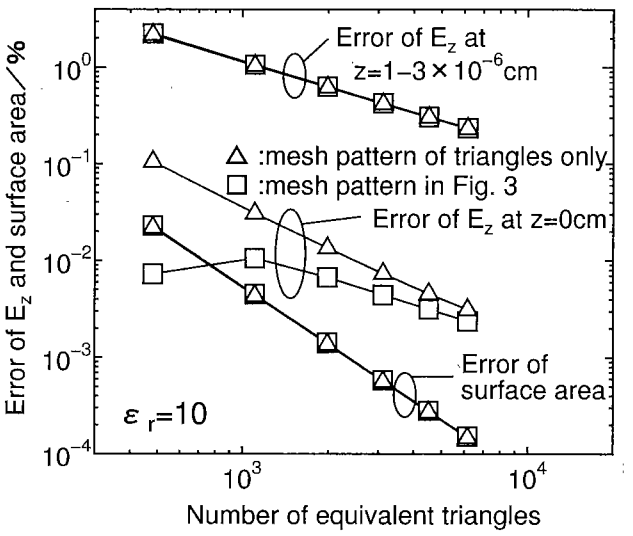

Fig. 5 Error of electric field strength and spherical surface area in relation to the number of equivalent triangles for a spherical dielectric.

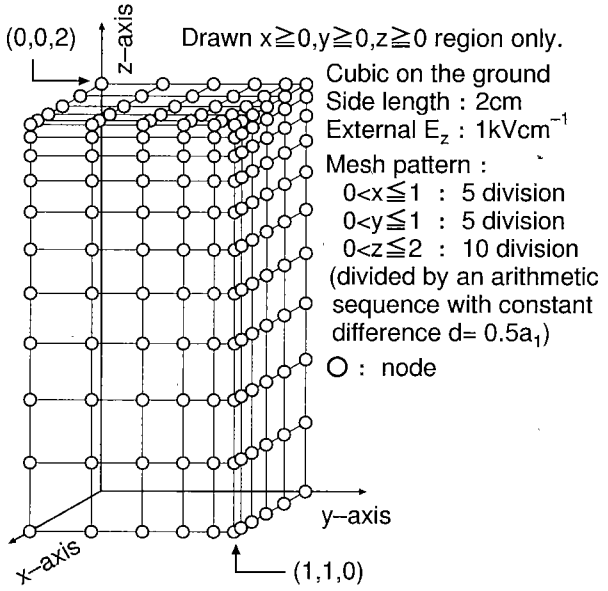

Fig. 6 Mesh pattern for a cubic dielectric on the ground.

The number of equivalent triangles ranges from 480 to 6160. The figure also shows the results corresponding to mesh patterns made by dividing a quadrilateral into two triangles. As additional information, the surface area errors of simulated surfaces are also plotted in the figure. Fig.5 indicates that the calculated results are reasonable and have enough accuracy in general use.

3.2 **Cubic dielectric** As a next benchmark example, we calculate the electric field for a cubic dielectric placed on the ground under a homogeneous field. As for this example, no analytical solution exists, so that the examination of the calculated results is a difficult matter. Furthermore it is known that the edge shape gives singular characteristics for the tangential component of electric field. In general, these characteristics make the accurate calculation difficult.

The side length of the cubic, the relative permittiv-

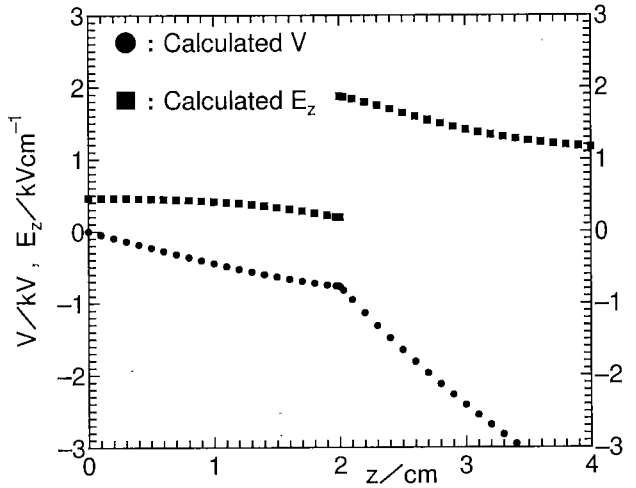

Fig. 7 Calculated potential V and field strength E_z on the z-axis for a cubic dielectric on the ground.

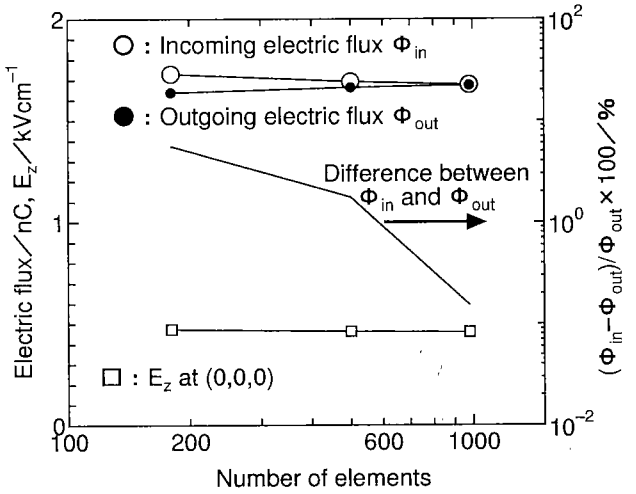

Fig. 8 Electric field and electric flux in relation to the number of elements for a cubic dielectric on the ground.

ity, and the homogeneous electric field strength are 2cm, 10, and 1kVcm^{-1} respectively. The homogeneous electric field is applied parallel to the z-axis. An example of applied mesh patterns is shown in Fig. 6. The division intervals are defined by using an arithmetic sequence with a constant difference d that equals a half of the first term of the sequence. The element width becomes narrower with approaching the edge part. The number of division is 10 over a side of the cubic, and the number of elements is 500 over the entire surface above the ground for the model shown in Fig. 6. Fig. 7 shows the calculated potential V and electric field E_z on the z-axis corresponding to the mesh pattern of Fig. 6. In order to estimate the validity of the calculated result, we have calculated both the electric flux Φ_{in} incoming through the bottom of the cubic and the flux Φ_{out} outgoing through the outer surface of the cubic. These two fluxes must theoretically agree with each other, so that the check of the agreement permits evaluating the degree of satisfaction of the necessary condition. Fig. 8 shows the calculated electric flux and field in relation to the number of surface elements. The number of elements is 180, 500, and 980 from left to right. The figure also represents the relative difference of Φ_{in} and Φ_{out}. Fig.8 shows that the calculated results at least satisfy the necessary condition with difference less than several percent.

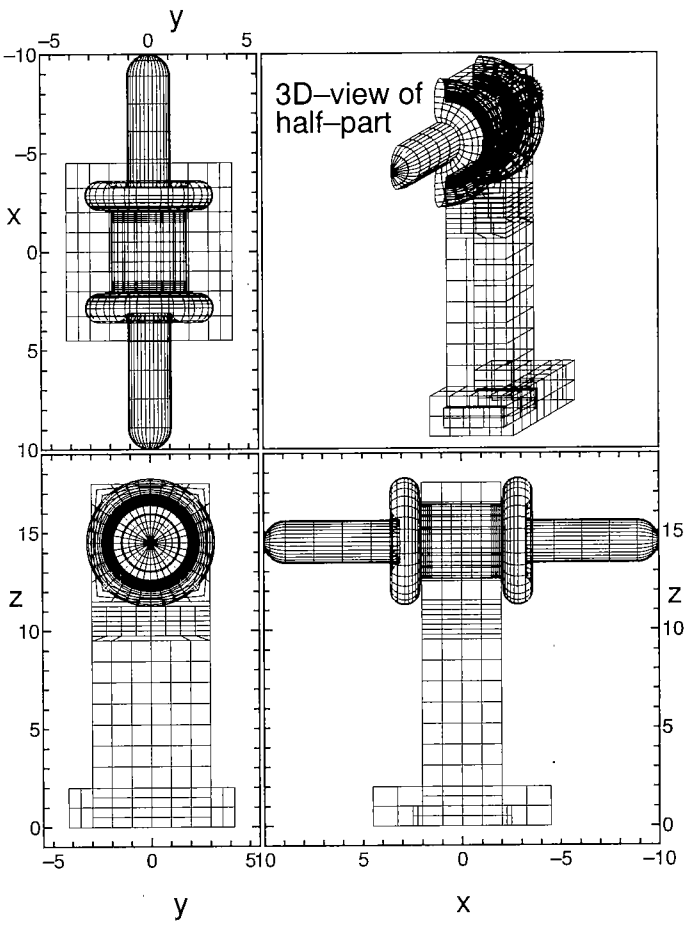

Fig. 9 A dielectric support of a high voltage feed line.

Table 1 Chief specifications of the support model.

Dielectric column	Relative permittivity=9.3
Height	17.5cm
Width	6.0cm
Depth	4.0cm
Feed line	Applied volt.=−100kV
Radius (in dielectric)	1.9cm
Radius (in vacuum)	1.1cm
Guard ring	Applied volt.=−100kV
Major radius	2.5cm
Minor radius	0.75cm
Metallic base	Grounded (0kV)
Height	2.0cm
Width	8.4cm
Depth	9.0cm

3.3 **Dielectric support** As a practical example, we calculate the electric field for a dielectric support of a high voltage feed line, which is used in vacuum as a component of a high energy accelerator. In this case, there appear curved surfaces, edge parts of the shape,

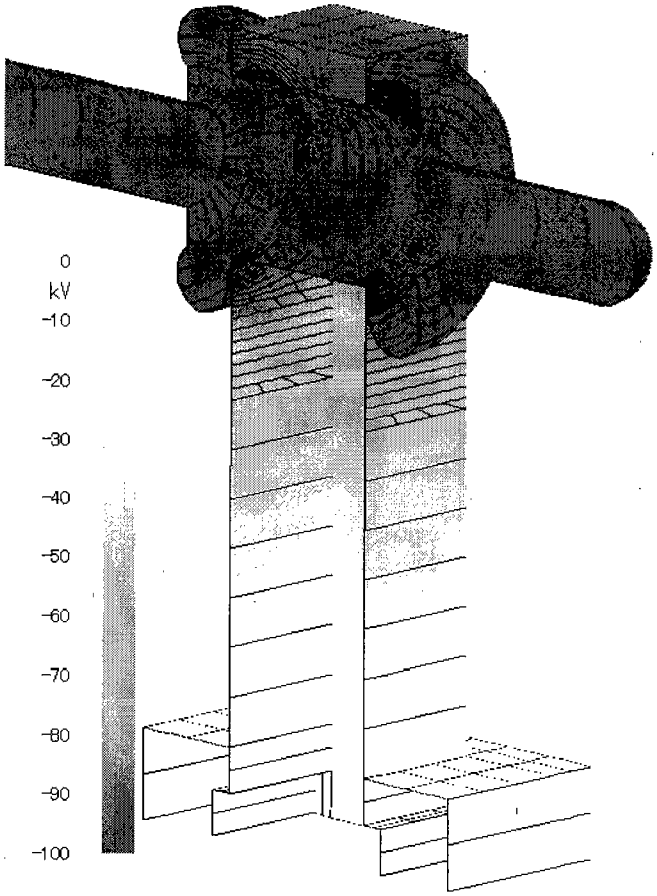

Fig. 10 Calculated potential distribution on the surface.

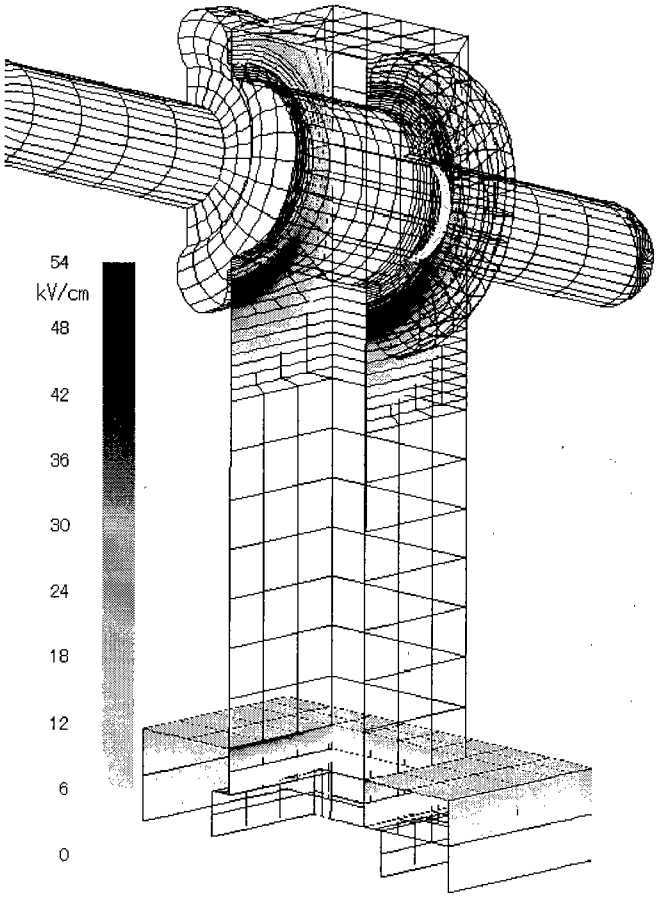

Fig. 11 Calculated distribution of normal component of field E_n on the surface (painted $E_n \geq 0$ region only).

and triple junctions of different materials. These surfaces or interfaces and the complex 3D shape make the field calculation difficult in general. On the other hand, it makes the condition advantageous to the calculation by SCM that an electric potential is fixed on the conducting boundary.

Fig. 9 shows the mesh pattern of the dielectric support. The model is composed of three parts. The feed line is a high-voltage (-100kV) conductor, and has two guard rings at both parts in contact with the dielectric support. The dielectric support is a rectangular solid with a hole, and the feed line penetrates the hole. The metallic base is a grounded holder of the dielectric support. Chief specifications for the model are listed in Table 1. It should be noted that the calculation model is simplified from the real equipment on several points. For example, the feed line is cut off and rounded at both ends for the convenience of calculation. The relative permittivity of the support is roughly estimated to be 9.3. The symmetric property at $y = 0$ plane is taken into consideration, and the number of used elements is 1842 for the half region. The quadrilateral elements are adopted in most of the surfaces, but triangular elements are partly used, for example, at the ends of the feed line.

Fig. 10 shows the calculated potential distribution on the all elements by shading the picture. It is clearly shown that the potential gradually varies from -100kV to 0kV. Fig. 11 shows the calculated distribution of normal component of field E_n on the surface. To simplify the figure, the shading is performed where E_n is directed outwardly from the surface. The normal component $\boldsymbol{E}_n$ on the dielectric is enhanced near the feed line and the guard rings as expected. However the strongest normal field, 54.1kVcm^{-1} at (x, y, z)=(2.0, 0.0, 11.84)cm, is observed at the region slightly apart from the high voltage conductor, (2.0, 0.0, 12.3)cm. It is because the guard rings are well working as for a field-relaxation role.

Fig. 12 shows the calculated distribution of electric field strength $|\boldsymbol{E}|$ on the $y = 0$ plane. The boundary between the feed line and the dielectric support is on both the line of $0 \leq x \leq$2cm, $z =$ 12.6cm and that of $x =$ 2.0cm, $12.3 \leq z \leq$ 12.6cm. The boundary between the dielectric support and the vacuum is on the line of $x =$ 2.0cm, $10.0 \leq z \leq$ 12.3cm. In the figure, the fields on the $x =$ 2.0cm boundary line are doubly plotted corresponding to the discontinuity of the field, by calculating them at $x = 2.0 \pm 10^{-5}$cm. An exact numerical treatment is impossible for the field at the triple junction, (2.0, 0.0, 12.3)cm, because it becomes infinitely high theoretically. However, compared with the ambient field strength, the calculated field of 144kVcm^{-1} at a point $(2.0 - 10^{-5}, 0.0, 12.3)$cm shows a qualitatively likely tendency of field enhancement in the vicinity of the singular point. The maximum field strength, except

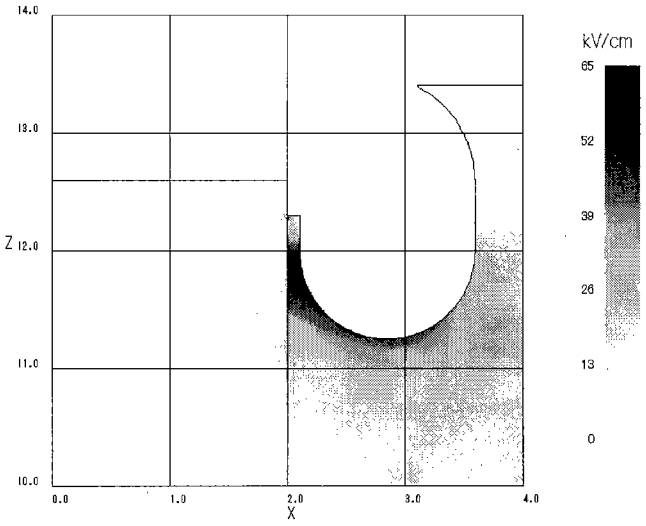

Fig. 12 Calculated distribution of field strength $|E|$ on $y = 0$ plane.

for the field at the triple junction, is $61.9\mathrm{kVcm}^{-1}$ on the surface of the guard ring at $(2.13, 0.0, 11.81)$cm.

4. Conclusion

An improved SCM is developed and tested, which analyzes the electric field in composite dielectrics in a three-dimensional arrangement. In this SCM, curved boundary surfaces are represented by third-order shape representation functions, and surface charge density distributions on the surfaces are expressed by non-conforming first-order charge representation functions. The contents of the paper are summarized as follows.

(1) Calculation methods of interior control points of the Bézier patch are formulated for the Zienkiewicz triangular and the Serendipity quadrilateral patches in order to represent curved surfaces.

(2) Non-conforming representation of charge density and the arrangement of matching points are designed in order to represent surface charge density and to obtain a set of discrete boundary equations.

(3) Two benchmark calculations of electric field are carried out relating to a spherical and a cubic dielectric. The calculated results confirm the validity of the present method.

(4) As a practical example, a field analysis has been carried out relating to a dielectric support of a high-voltage feed line to obtain the field distribution, in particular, to specify the strongest field region on the surface.

From these calculation results, we could confirm the usefulness of the proposed SCM for computing electric fields in complicated 3D arrangements.

(Manuscript received December 25, 2000, revised April 18, 2001)

References

(1) S. Hamada and T. Takuma: Electric field calculation in composite dielectrics by first-order triangular surface charge method, T. IEE Japan, Vol. 120–A, No. 4, pp.445–450 (2000)(in Japanese)

(2) S. Hamada, B. Techaumnat and T. Takuma: Electric field calculation in composite dielectrics by curved triangular surface charge method, T. IEE Japan, Vol. 120–A, No. 5, pp.568–574 (2000)(in Japanese)

(3) B. Y. Lee, S. H. Myung et al.: "The Use of Rational B-Spline Surface to Improve the Shape Control for Three Dimensional Insulation Design and Its Application to Design of Shield Ring", IEEE Trans. PWRD., Vol. 13, No. 3, 962–968(1998)

(4) C. Vetter and H. Singer: "High-voltage field computation using bi-cubic surface splines", High Voltage Engineering Symposium, 22–27 August 1999, Conference Publication No. 467, IEE, 1999

(5) M. Hosaka: "Modeling of curves and surfaces in CAD/CAM", Springer-Verlag Berlin Heidelberg (1992)

(6) R. E. Barnhill and R. F. Riesenfeld: "Computer aided geometric design", Proceedings of a conference held at the University of Utah, Salt Lake City, Utah, March 18-21, 1974, Academic Press (1974)

(7) O. C. Zienkiewicz: "The finite element method", McGraw-Hill(1977)

(8) H. Tsuboi and T. Takayama: "Setting up curved surface triangular element for boundary element method", IEEJ Tech Rep. on SA and RM, SA-97-15 / RM-97-74, Aug. 1997. (in Japanese)

(9) G. R. Cowper: "Gaussian quadrature formulas for triangles", International Journal for Numerical Method in Engineering, **7**, 405–408(1973)

Shoji Hamada (Member) He was born on February 13, 1965. He received the B. S. degree from Kyoto University in 1987 and the M. S. and Dr. degrees in electrical engineering from the University of Tokyo in 1989 and 1992, respectively. He worked with the Tokyo Denki University from 1992 to 1997. Since 1997 he is Lecturer at the Department of Electrical Engineering, Kyoto University. He has been engaged in the studies of electrical discharges and electric field calculation.

Tadasu Takuma (Member) He was born in Mie Prefecture, Japan, on September 30, 1938. He received his B. S., M. S., and Ph. D. degrees in electrical engineering from the University of Tokyo in 1961, 1963 and 1966, respectively. After one-year service as Lecturer of Electrical Engineering in the University of Tokyo, he joined CRIEPI in 1967. Since February 1995, he is Professor at the Department of Electrical Engineering, Kyoto University. He has been engaged in the study of SF_6 gas insulation, gas discharge, environmental problems of transmission lines and numerical field calculation.

Yoshio Saitoh (Member) Yoshio Saito was born on June 10, 1951. He studied applied physics at the University of Tokyo, and received the Ph.D. degree from the Faculty of Engineering of the University of Tokyo, in 1979. In 1980, he joined High Energy Accelerator Research Organization (KEK). His main research interest is discharge phenomena in vacuum.